Liu *et al. Advances in Aerodynamics* (2023) 5:7
https://doi.org/10.1186/s42774-022-00136-8

Advances in Aerodynamics

RESEARCH Open Access

On the drag reduction mechanism of hypersonic turbulent boundary layers subject to heated wall blowing

Qiang Liu[1], Zhenbing Luo[1*], Yan Zhou[1], Wei Xie[1] and Siwei Dong[2]

*Correspondence:
luozhenbing@163.com

[1] College of Aerospace Science and Engineering, National University of Defense Technology, Changsha 410073, China
[2] State Key Laboratory of Aerodynamics, Mianyang 621000, China

Abstract

Turbulence drag reduction is of great significance for the range increase of hypersonic flight vehicles. The proposed velocity-temperature coupling control method (Liu et al, Phys Rev Fluids 6:044603, 2021) is further extended to the hypersonic turbulent boundary layer. Direct numerical simulation results of four comparative cases show that the heated wall blowing achieves a drag reduction rate of 10.58%, which is about the sum of wall blowing (5.27%) and wall heating (6.35%). By evaluating the control efficiency, however, it is found that heated wall blowing is not as good as wall blowing and cannot obtain net energy saving rate. The modified FIK decompositions of skin friction coefficient indicate that the cliffy decrease of the mean convection term is the primary contribution for the drag reduction. Effects of the proposed control measure on turbulence statistics and coherent structures are also analyzed. Streamwise vortex is found to be away from the wall, thus leading to a lower friction drag.

Keywords: Hypersonic turbulent boundary layer, Turbulence drag reduction, Velocity-temperature coupled control, Turbulence statistics, Turbulence structures, Direct numerical simulations

1 Introduction

Compared with laminar flow, the friction of turbulent boundary layers (TBL) is usually increased by a factor of 3-5 [1]. Studies have shown that for a subsonic aircraft in cruise state, the friction drag of turbulent boundary layer accounts for 50% of the total drag, and every 1% reduction in drag can reduce fuel consumption by 0.75% [2]. Even under flight conditions dominated by shock drag in a supersonic/hypersonic flow, the turbulent friction drag still accounts for about 30% of the total drag [3, 4]. Therefore, using appropriate flow control techniques to achieve the drag reduction of the turbulent boundary layer will greatly increase the range of the hypersonic flight vehicle under the same fuel consumption, which is of great significance for reducing the carbon emission content as well.

Generally, flow control techniques can be divided into passive and active ones, depending on whether energy consumption is required [2]. Riblet is believed to be one of the most popular and mature passive control measures in turbulence drag reduction [5, 6]. There are

Springer Open

© The Author(s) 2023. **Open Access** This article is licensed under a Creative Commons Attribution 4.0 International License, which permits use, sharing, adaptation, distribution and reproduction in any medium or format, as long as you give appropriate credit to the original author(s) and the source, provide a link to the Creative Commons licence, and indicate if changes were made. The images or other third party material in this article are included in the article's Creative Commons licence, unless indicated otherwise in a credit line to the material. If material is not included in the article's Creative Commons licence and your intended use is not permitted by statutory regulation or exceeds the permitted use, you will need to obtain permission directly from the copyright holder. To view a copy of this licence, visit http://creativecommons.org/licenses/by/4.0/.

two main viewpoints on the drag reduction mechanism of riblets: Suzuki and Kasagi [7] found that momentum transport is enhanced by secondary vortices, and the drag reduction mechanism of the riblets is considered to be the inhibition of vortex generation in the near-wall region and the eddy dissipation caused by the redistribution of turbulent kinetic energy from the streamwise component to the spanwise component; Choi, Moin and Kim [8] believed that the riblets can limit the position of the streamwise vortex to the upper part of the riblets, resulting in only limited part of riblets being exposed to the downwash motion of the high-speed fluid, while for the drag-increasing riblets, the flow vortex often invades into the valley, bringing a high shearing stress to the wall. Robinson [9] was the first to carry out the wind tunnel experiments of supersonic flat-plate with riblets wall. The Mach number was 2.97, and the drag reduction rate achieved was 4%. Gaudet [10] studied the flow at Mach 1.25 and achieved a 7% drag reduction rate on the riblet surface, compared to the smooth wall. Coustols and Cousteix [11] conducted wind tunnel experiments at free-stream Mach numbers of 1.6, 2.0, and 2.5, and achieved a maximum drag reduction rate of 4%. Duan and Choudhari [3, 12] conducted direct numerical simulations (DNS) of the boundary layer of a flat plate with zero-pressure-gradients with Mach numbers 2.5 and 7.2 controlled by symmetrical V-shaped riblets, and found that when the dimensionless spanwise peak-to-peak spacing of the riblets is $s^+ = 20$, the turbulence intensity and Reynolds stress can be greatly reduced, and a drag reduction of about 7% can be obtained. At the same time, they also studied the effect of riblets on the heat transfer characteristics of the wall, only to find that the Reynolds analogy factor is approximately equal to that on the smooth wall [3]. Chen [13] studied the effect of the streamwise riblets on the drag reduction of a Mach 6 hypersonic TBL, and found that it can reduce the contribution of the turbulent contribution term to the skin friction. As a result, a drag reduction rate of about 7% was obtained. Based on the work [13], Zhou et al. [14] further studied the effect of riblet height h_w and spanwise wavelength λ_w on the Mach 6 turbulent boundary layer, and found that within a certain range, the drag reduction rate is proportional to height but varies inversely with the spanwise wavelength.

Active flow control techniques for drag reduction of the supersonic/hypersonic TBL involve wall blowing/suction, wall heating/cooling, etc. Kametani et al. [15] studied the effect of uniform blowing/suction on supersonic turbulent channel flow at Mach 1.5, and the drag reduction rate was up to 10.3%. Chen et al. [16] studied the control effect of the uniform blowing on the drag reduction of the Mach 6 hypersonic turbulent boundary layer. With a blowing amplitude of 0.3% of freestream velocity, the friction drag is reduced by about 42%, which is mainly due to the drop of the average viscous shear stress. Through the modified FIK (Fukagata, Iwamoto & Kasagi) decomposition analysis, it is found that the subsidence of the skin friction coefficient is mainly due to the decrease of the average convection term, while the high Reynolds stress brought by the turbulence amplifications does not play a decisive role in the increase or decrease of the friction.

Also, numerous studies have been conducted on the effect of wall temperature on hypersonic turbulent boundary layers. Duan et al. [17] studied the effect of wall temperature T_w on the Mach 5 hypersonic turbulent boundary layer with T_w/T_δ (T_δ is the temperature at the outer edge of the boundary layer) varying between 1 and 5.4, and found that the cooling wall enhanced the coherence of the near-wall flow structures and vorticities. Huang et al. [18] investigated the effect of cold wall ($T_w/T_r = 0.2$, T_r is the recovery

temperature) on turbulent flow characteristics at high Mach numbers ($Ma = 11$ and 14) and high friction Reynolds number ($Re_\tau = 1200$). Liang and Li [19] investigated the effects of Mach number and wall temperature on compressible turbulent boundary layers by evaluating the compressibility effect and strong Reynolds analogy (SRA), and showed that Morkovin's hypothesis [20] is still valid even to Mach number of 8. Li et al. [21] investigated the relationship between the fluctuating density and fluctuating temperature in the Mach 8 hypersonic TBL with different wall temperatures. The results show that the cold wall has an inhibitory effect on the extreme events of wall turbulence, and the correlation radius of the coherent structure near the wall increases. Xu et al. [22] carried out Helmholtz decomposition of hypersonic turbulent boundary layers at different wall temperatures, and found that cold wall would enhance the dilation term of the Reynolds normal stress in the near-wall region.

Although the whole wall temperature has an effect on the skin friction coefficient, the high energy consumption also makes it difficult to generate net energy saving rate [23], which seriously affects the practical application of wall temperature control. To this end, more efficient drag reduction control strategies need to be developed. Gad-el-Hak pointed out that drag reduction can be achieved by changing the local flow rather than the overall flow, which is called "targeted control" [2]. Unlike the wall temperature (cold wall, adiabatic wall, hot wall) that affects the entire boundary layer, local wall heating/cooling is achieved by arranging local heating/cooling strips on the wall, and its control amplitude is relatively small. Zhang et al. [24] carried out a numerical simulation study of compressible turbulent boundary layer control based on local wall heating. The results show that the turbulent activity near the wall is suppressed and the skin friction drag is reduced. Hickey et al. [25] arranged several heating strips distributed alternately in the spanwise direction in a compressible channel turbulence, and the spacing of the strips was obtained by semi-empirical mode decomposition. It is demonstrated that the decrease of the average density leads to a more considerable reduction in the wall friction, and the drag reduction rate with an optimal heating strip reaches 6%.

To achieve a better drag reduction effect, breaking through the defects of a single flow control technique and developing a new turbulence drag reduction method combining multiple means will become a research hotspot. Recently, the author proposed a novel velocity-temperature coupled control method using wall heating blowing, which had been applied on supersonic TBLs [26, 27]. This method couples the advantages of traditional wall blowing and wall heating control. The direct numerical simulations show that a moderate increase of gas temperature of the wall blowing (relative to the wall temperature) can achieve a higher drag reduction rate (20.1%) while maintaining the net energy saving rate when coupled velocity-temperature control is applied, which is the sum of the drag reduction ratios of wall blowing (7.4%) and wall heating (14.1%). The Renard-Deck decomposition of the skin friction coefficient [28] shows that the significant reduction in the spatial growth term is an important contribution to the drag reduction.

As we can see, there are not many studies on drag reduction for hypersonic TBL due to the fact of much more challenges and difficulties in both simulations and experiments. However, turbulence drag reduction under hypersonic conditions has more important engineering value for breaking through the bottleneck of range extension and energy

saving for hypersonic flight vehicles. In this paper, we will extend the proposed velocity-temperature coupled control method to hypersonic turbulent layer, verify and compare the control effect via DNS. Effect on skin friction coefficients, turbulence statistics and flow organization are mainly discussed to reveal the control mechanism.

2 Numerical setups

2.1 Freestream conditions and control parameters

This paper proposes a velocity-temperature coupled control method for the drag reduction of hypersonic turbulent boundary layers over a sharp leading-edge flat plate. The freestream conditions (variables with subscript "∞") are taken from the wind tunnel FD-7 of China Aerospace Aerodynamics Research Institute, with Mach number $Ma_\infty = 6$, static temperature $T_\infty = 54.9$ K, and unit Reynolds number $Re_\infty/\text{mm} = 2.0 \times 10^4$. The flat plate is isothermal, with the wall temperature T_w equal to the wall recovery temperature $T_r = T_\infty(1 + r((\gamma - 1)/2)Ma_\infty^2)$, where the recovery factor $r = \sqrt[3]{Pr}$, the molecular Prandtl number Pr and specific heat ratio γ are respectively 0.72 and 1.4. The viscosity is calculated by Sutherland's law.

As shown in Fig. 1, the velocity-temperature coupled control is realized by blowing heated ejections from six streamwise-aligned slots on the wall. These slots, 1000 mm downstream of the inlet, are equidistantly distributed in the spanwise direction with a distance of $\Delta z^+ = 52$ (variables with superscript "+" are normalized by wall units), roughly half the distance between high- and low-speed streaks. The spanwise width of each slot is also equal to $\Delta z^+ = 52$. Note that different spacing and widths of the streamwise-aligned slots have been investigated in a previous paper [26], only to find that the drag reduction rate is independent of these parameters.

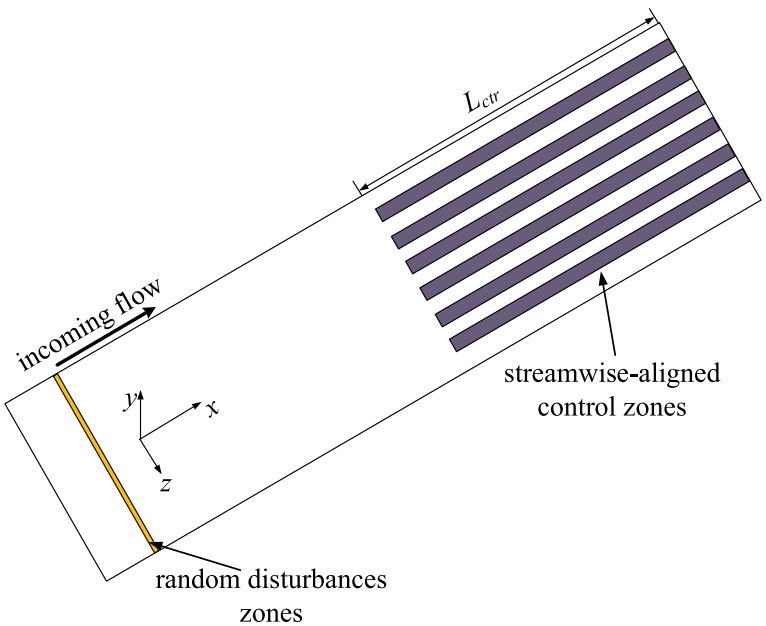

Fig. 1 Schematic of hypersonic flat-plate with streamwise-aligned control zones (each slot is equidistant from the other)

Four cases with different combinations of wall-normal blowing amplitude v_b and slot temperature T_{slot} are conducted. Control parameters are shown in Table 1. The amplitude of the ejections from these slots is $v_b = 0.1\%u_\infty$. These ejections are either isothermal with $T_{slot}/T_w = 1$ or heated with $T_{slot}/T_w = 1.01$. Note that the temperature amplitude is ten times of the blowing amplitude, because the drag reduction effect is weak if the temperature amplitude is too small.

2.2 Numerical setups

Figure 2 presents a sketch of the numerical simulation. The streamwise, wall-normal and spanwise directions are respectively represented by x, y and z. The computational domain, with a size $(L_x, L_y, L_z)/\text{mm} = (1310, 36, 30)$, is discretized by a grid size $(N_x, N_y, N_z) = (4482, 155, 256)$, yielding a total of 0.145 billion grid points. In the streamwise direction, the grid is densified uniformly ranging from $x = 800$ mm to $x = 1320$ mm. The resulting grid resolutions (shown in Table 2) in the streamwise and spanwise directions are respectively $\Delta x^+ = 6.3$ and $\Delta z^+ = 3.7$. The "+" represents dimensionless in wall units. The wall-normal resolutions measured at the wall and boundary layer edge are respectively $\Delta {y_w}^+ = 0.47$ and $\Delta {y_\delta}^+ = 8.5$. Compared with other DNS studies [17, 19], our resolutions are sufficient to capture small-scale structures.

Random disturbances by wall blowing and suction [29] are introduced to generate fully-developed compressible turbulent boundary layers by bypass transition. The given disturbance amplitude A is 0.15, and the frequency β is set to 44.5 kHz. The disturbance zone ranges from 150 mm to 200 mm. The whole flow field is initialized by the incoming flow.

Table 1 Control parameters

Case	Δv	ΔT
NC	0	0
B1H1	0.1%	1%
B1	0.1%	0
H1	0	1%

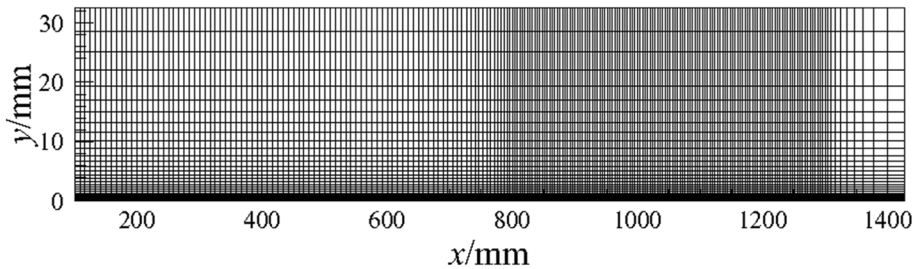

Fig. 2 Schematic of computational mesh

Table 2 Computational parameters and mesh scales in NC case at $x = 1000$ mm

Ma_∞	Re_∞/mm	(L_x, L_y, L_z)/mm	N_x, N_y, N_z	Δx^+	$\Delta {y_w}^+$	Δz^+
6	2.0×10^4	$1310 \times 36 \times 30$	$4482 \times 155 \times 256$	6.3	0.47	3.7

Compressible three-dimensional Navier-Stokes equations in the form of total energy are solved using an open-source direct numerical simulation software OpenCFD developed by Li, which has been widely used in the numerical simulations of transitional and turbulent compressible boundary layers [30, 31]. Convection terms are resolved by the Steger-Warming splitting method, combining with a seventh-order weighted essentially non-oscillatory (WENO-SYMBO) scheme, whereas the viscous terms are solved by an eighth-order central finite-difference scheme. Time is advanced with a third-order total variation diminishing (TVD) Runge-Kutta method.

Two average methods are introduced for turbulence statistics: one is the Reynolds average, which regards turbulence signal f as the superposition of average signal $<f>$ and fluctuating signal f', namely, $f = \overline{f} + f'$, where superscript '-' denotes the time average of turbulence signal. The other is the Favre average considering density correction, in the form of $f = \tilde{f} + f''$, with $\tilde{f} = \overline{\rho f} \Big/ \overline{\rho}$, where superscript '~' denotes the density-weighted average of turbulence signal. The flow field reaches a statistical stationary state after 5000 dimensionless time (δ/u_∞, $\delta = 1$ mm), and then a total of 2000 samples are collected for statistical analysis with a time interval of 1.2 δ/u_∞.

2.3 Validation

Before proceeding to the control performance, this section provides validation of DNS results by comparing with other DNS studies. Figure 3 plots the streamwise development of the skin-friction coefficient defined by

$$C_f = 2\tau_w \Big/ \rho_\infty u_\infty^2 \tag{1}$$

in comparison with the theoretical estimated profile given by White [1],

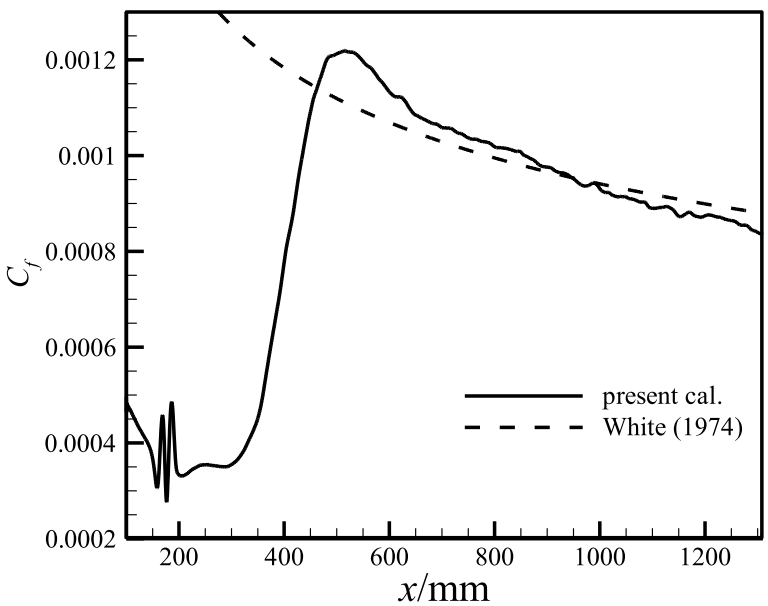

Fig. 3 Skin friction coefficient along the streamwise direction and White law [1]

$$C_f = \frac{0.455}{S^2}\left[\ln\left(\frac{0.06}{S}Re_x\frac{1}{\overline{\mu}_w}\sqrt{\frac{1}{\overline{\overline{T}}_w}}\right)\right]^{-2}, \tag{2}$$

where

$$S = \frac{1}{\arcsin A}\sqrt{\overline{T}_w - 1},\ A = \left(\frac{\gamma-1}{2}Ma_\infty^2\frac{1}{\overline{\overline{T}}_w}\right)^{1/2}, \tag{3}$$

x is the distance from the leading edge of the flat-plate, and $\overline{\mu}_w$ and $\overline{T}_w$ are respectively the mean viscosity and temperature of wall. It can be seen that the skin friction coefficient rapidly climbs to the peak with the transition of boundary layer, and quickly returns to an equilibrium state after a short overshoot. In the fully developed turbulence zone, the calculated values are in good agreement with the theoretical ones (scattered by the triangle symbol), which declares the accuracy of the simulation results.

Figure 4 shows the van Driest transformed mean streamwise velocity in the fully-developed zone ($Re_\theta = 8000$). For comparison, the result of Duan et al. [17] is also redrawn in the figure. Under the condition of adiabatic wall temperature, the mean velocity profile is in good agreement with the results of Dual et al. [17] and the classical wall law, in which the slope κ of the logarithmic law region is 0.41 and the value of the intercept C is confined to 5.2. It should be noted that the seventh-order WENO (WENO7) scheme is adopted at first, only to find that WENO7 has large dissipation, resulting in a higher value of C (up to 5.9) and higher skin friction coefficient. After several tests, the WENO-SYMBO with lower numerical dissipation is selected finally.

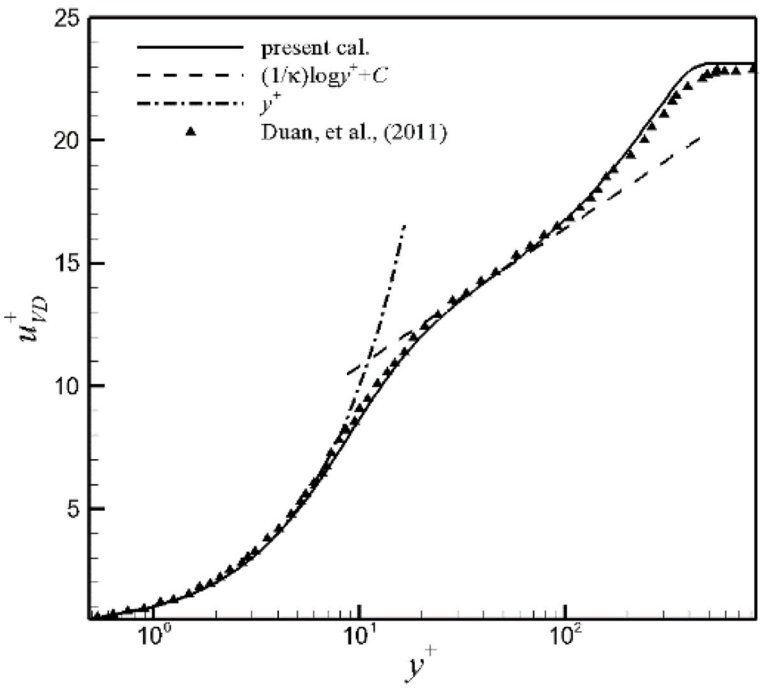

Fig. 4 Profile of van Driest transformed mean velocity obtained at $Re_\theta = 8000$ [17]

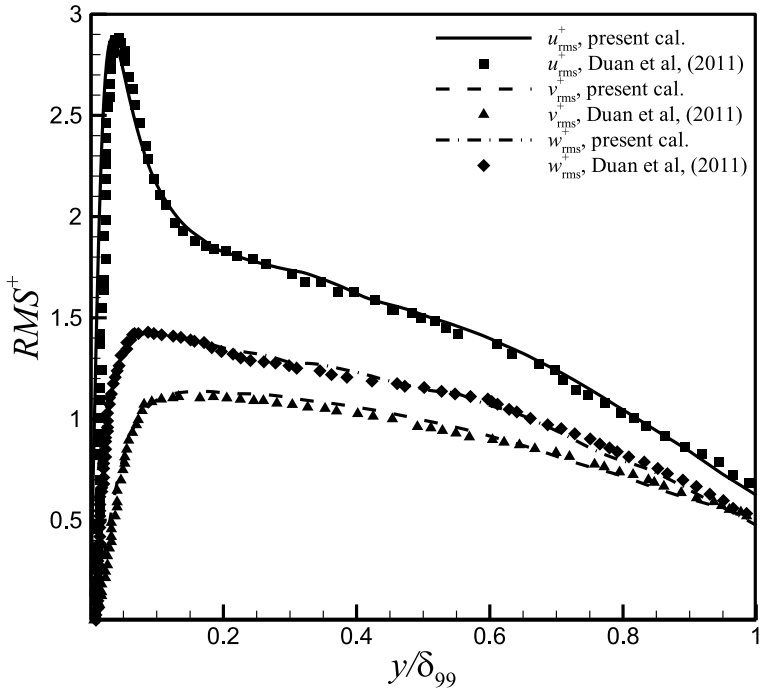

Fig. 5 Turbulence intensity versus Morkovin's scaling at $Re_\theta = 8000$

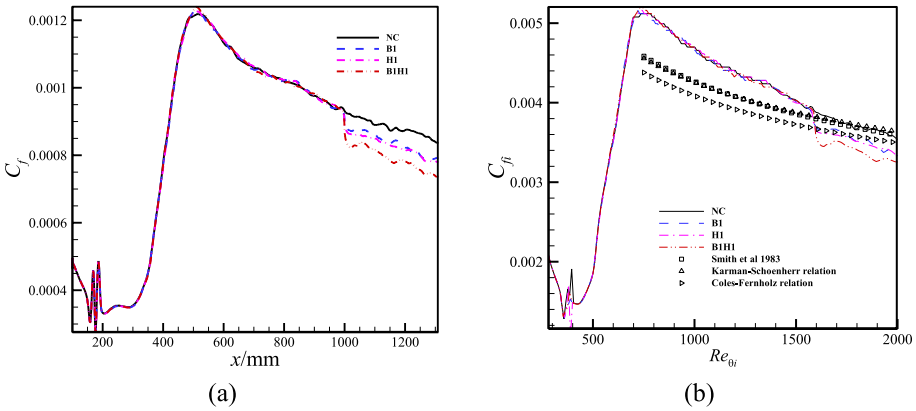

Fig. 6 Skin friction coefficient versus x (**a**) and $Re_{\theta i}$ (**b**) in each case

Figure 5 gives the wall-normal profiles of turbulence intensities in three directions versus Morkovin's scaling at $Re_\theta = 8000$. One can see that our results are in good fit with the results of Duan et al. [17] in both inner and outer boundary layers, which fully proves the accuracy of the grid and numerical settings in this paper.

3 Results and discussions

3.1 Effect on skin friction coefficients

First, the variations of the skin friction coefficients along the flow direction controlled with different measures are demonstrated in Fig. 6a. As shown in the figure, after the wall blowing (B1) and the wall heating (H1) control are respectively applied, the wall friction is reduced, and the drag reduction effect of the latter is better than that of the former. When

the velocity-temperature coupling control (heated wall blowing, B1H1) is applied, the skin friction coefficient is greatly reduced. For quantitative comparison, drag reduction rate *DR* is introduced, which is defined as

$$DR = \frac{C_{f,nc} - C_{f,ctr}}{C_{f,nc}}, \tag{4}$$

$$C_{f,nc(ctr)} = \frac{1}{L_{ctr}} \int_0^{L_{ctr}} c_{f,nc(ctr)}(x)dx, \tag{5}$$

where the subscripts *nc* and *ctr* denote without and with flow control, respectively. L_{ctr} is the streamwise length of the control zone. This means that the *DR* is calculated by the global friction coefficient in the whole control zone. Table 3 shows the drag reduction rate under different control methods. In the B1 case, the drag reduction rate is 5.27%, and in the H1 case, the drag reduction rate is 6.35%, which is about 1.2 times higher than that of the wall blowing. After the velocity-temperature coupling control is applied, the drag reduction rate is greatly improved, reaching as high as 10.58%, which is almost the sum of the drag reduction effects of wall blowing and wall heating. Even under hypersonic conditions, the drag reduction control method of TBL based on heated wall blowing can still achieve the superposition effect of wall blowing and wall heating. However, compared with the results in supersonic TBL [26], the drag reduction efficiency of wall blowing/heated wall blowing is greatly reduced under hypersonic conditions, and the drag reduction rate is almost reduced by half, which is due to the strong compressibility of the hypersonic turbulent boundary layer. The strong compressibility of the main flow suppresses the wall-normal fluctuating velocity of the turbulent boundary layer, which weakens the "virtual wall" effect produced by the flow control method.

According to Morkovin's hypothesis, the theory of compressible turbulence is similar to that of incompressible one through density-weighted correction [20]. The van Driest II transformation [32] can be adopted to transform the skin friction coefficient and momentum Reynolds number of compressible boundary layer into incompressible parameters, expressed as

$$C_{fi} = F_c C_f, \quad Re_{\theta i} = \mu_\infty / \mu_w Re_\theta, \tag{6}$$

$$F_c = \frac{T_w/T_\infty - 1}{\arcsin^2 \alpha}, \quad \alpha = \frac{T_w/T_\infty - 1}{\sqrt{T_w/T_\infty (T_w/T_\infty - 1)}}, \tag{7}$$

Table 3 Drag reduction rates with different control measures

Case	B1	H1	B1H1
DR	5.27%	6.35%	10.58%

where i denotes incompressible. Figure 6b presents the variation of skin friction coefficients with $Re_{\theta i}$. Typical relations from Smith et al. [33], Karman-Schoenherr [34], and Coles-Fernholz [35], as shown respectively in the following, are also drawn for comparison:

$$C_{fi} = 0.024 Re_{\theta i}^{-1/4}, \tag{8}$$

$$C_{fi} = \frac{1}{\log(2Re_{\theta i})[17.075\log(2Re_{\theta i}) + 14.832]}, \tag{9}$$

$$C_{fi} = 2[1/0.384\ln(Re_{\theta i}) + 4.127]^{-2}. \tag{10}$$

It can be seen that as the turbulent boundary layer gradually develops to the equilibrium state, the differences between the skin friction coefficient in NC and the relations of Smith et al. and Karman-Schoenherr decrease, but there is always an obvious difference with Coles-Fernholz relations.

As to the control efficiency, we introduce the gain G and input power W_{in}, which are defined in forms of

$$G = \frac{C_{f,nc} - C_{f,ctr}}{2W_{in}/\left(L_{ctr}\rho_e u_e^3\right)}, \tag{11}$$

$$W_{in} = \int_0^{L_{ctr}} \left[(P_w - P_{w-})v_b + \frac{1}{2}\rho_b v_b^3\right] dx + \frac{1}{RePr}\int_0^{L_{ctr}} \left|\overline{\frac{\partial T}{\partial y}}\right|_w dx, \tag{12}$$

where P_w and $P_{w\text{-}}$ denote the wall mean pressure and the mean pressure on the other side of the wall where wall blowing is applied, respectively, and ρ_b is the density of blowing gas. Here, the first term of W_{in} denotes the energy consumed by wall blowing while the second term denotes the energy consumed by heating. Then, we can get the net energy saving rate S, which is defined as

$$S = \frac{C_{f,nc} - \left(C_{f,ctr} + 2W_{in}/\left(L_{ctr}\rho_e u_e^3\right)\right)}{C_{f,nc}}. \tag{13}$$

Figure 7 draws the corresponding drag reduction benefit graphs under different control methods. The drag reduction results of the supersonic turbulent boundary layer in reference [26], opposing control by Choi [36], uniform blowing by Kametani [15], and steady streamwise near-wall force by Xu [37] are also shown in the figure. First, it is not difficult to see that the net gain under hypersonic conditions is lower than that under supersonic TBL, indicating that the strong compressibility reduces the control efficiency. After careful observation of each control method, it can be found that the simple wall blowing control (B1) still has higher control efficiency; although the heated wall control method has a higher drag reduction rate, the energy consumption required is also quite high (compared with the wall blowing), the net energy saving rate decreases and the control efficiency decreases. A careful observation of the net energy saving rate of heated wall blowing (B1H1) shows that it is lower

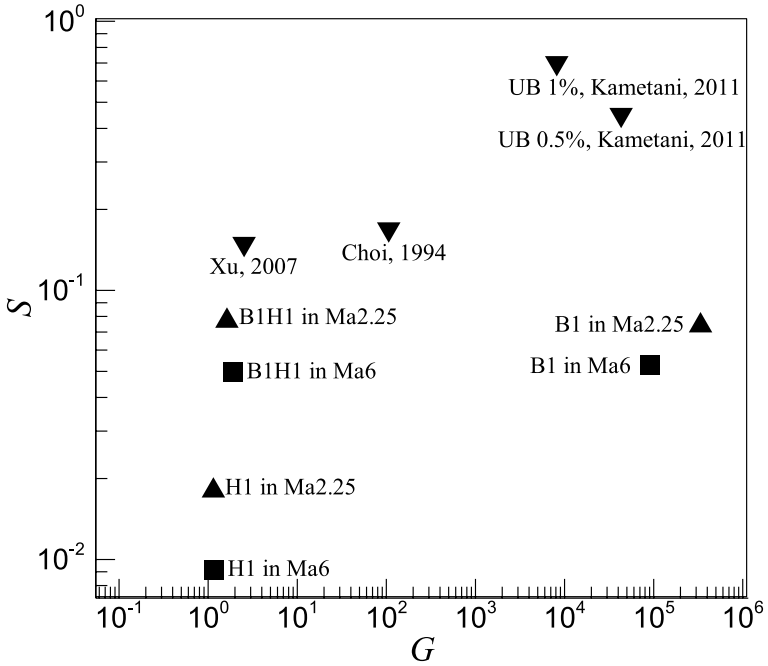

Fig. 7 Net energy saving rate *S* versus gain *G* and comparisons with other control measures

than that of wall blowing, indicating that the control efficiency of heated wall blowing is not as good as that of simple wall blowing, which is different with the conclusions in reference [27]. This may be because, under the condition of hypersonic incoming flow and high wall temperature ratio, the energy consumption required to achieve the heated wall blowing is much higher than that under the supersonic condition. On the other hand, the net energy saving rates of the control measures in this paper are significantly lower than others [15, 36, 37]. All in all, the above analysis shows that, in the hypersonic TBL, although the velocity-temperature coupled control method has a higher drag reduction rate, its control efficiency may not be as good as the wall blowing.

Referring to the work of Chen et al. [16], the modified FIK identity is used to decompose the friction coefficient of the hypersonic turbulent boundary layer, and its expression is as follows:

$$\begin{aligned} c_f(x) &= c_l(x) + c_t(x) + c_m(x) + c_c(x) + c_{ct}(x) + c_d(x) \\ &= \frac{4}{Re_\delta}(1-\delta_d) + 4\int_0^1 (1-y)\left(-\overline{\rho u'' v''}\right)dy \\ &+ 4\int_0^1 (1-y)(-\overline{\rho}\tilde{u}\tilde{v})dy + \frac{4}{Re_\delta}\int_0^1 (1-y)(\overline{\mu}-1)\frac{\partial \overline{u}}{\partial y}dy \\ &+ \frac{4}{Re_\delta}\int_0^1 (1-y)\left(\overline{\mu'\left(\frac{\partial u'}{\partial y}+\frac{\partial v'}{\partial y}\right)}\right)dy \\ &-2\int_0^1 (1-y)^2(\overline{I}_x)dy, \end{aligned} \tag{14}$$

where

$$\bar{I}_x = \frac{\partial\overline{(\rho u^2)}}{\partial x} - \frac{1}{Re_\delta}\frac{\partial\overline{\tau_{xx}}}{\partial x} - \frac{1}{Re_\delta}\frac{\partial}{\partial y}\left(\overline{\mu}\frac{\partial\overline{v}}{\partial x}\right). \tag{15}$$

In the above expression, δ_d is the dimensionless displacement thickness, C_l is the contribution term of laminar flow, C_t is the contribution term of turbulent flow, C_m is the contribution term of mean convection, C_c is the contribution term of compressibility, C_{ct} is the contribution term of the interaction between compressibility and turbulence, and C_d is the contribution term of spatial development of flow in the streamwise direction.

Figure 8 plots the histogram graph of the skin friction coefficient decomposition under different control methods. Note that a negative sign is added before C_m. It can be seen from the figure that in the uncontrolled case, the turbulent contribution term C_t, the average convective contribution term C_m and the spatial development of flow in the streamwise direction C_d are the main components of turbulent friction drag. The proportion of the laminar contribution term C_l and the compressible contribution term C_c is very small, and the proportion of the compressible and turbulent interaction contribution term C_{ct} is almost negligible.

After the three flow control techniques are applied, the mean convection term C_m is drastically reduced, which is the direct cause of the reduction in the turbulent friction coefficient. Due to the turbulence amplification effect and the increase of the thickness of the boundary layer (given below), the proportion of the turbulence contribution term C_t and the spatial development contribution term C_d increases, but its increasing effect is offset by the average convection term C_m, which eventually leads to a decrease in the skin friction coefficient. The laminar contribution term C_l is hardly affected. The contributions of the compressible term C_c and the compressible and turbulent interaction term C_{ct} are still small, but this does not mean that the effects of these two terms can be ignored. In fact, if the wall temperature continues to increase, they will not be ignored [13]. This shows that under the modified FIK friction decomposition framework, for the hypersonic flat-plate turbulent boundary layer controlled by (heated) wall blowing, the direct reason for the reduction of the skin friction coefficient is the reduction of the mean convective term. The increase in the turbulence contribution term due to turbulence amplifications is not decisive.

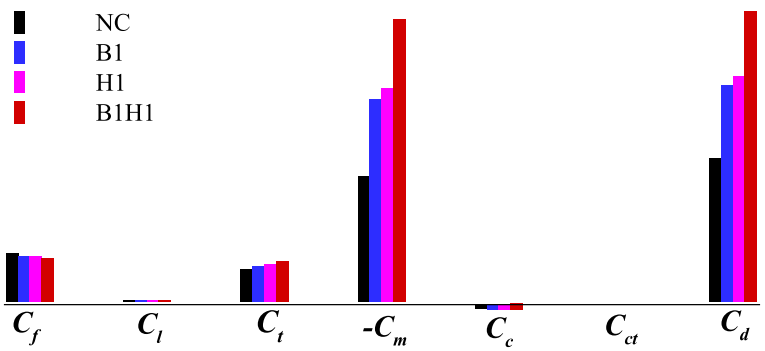

Fig. 8 Bar graph of each contribution term in C_f decomposition in each case

3.2 Turbulence statistics characteristics

Figure 9 plots the van Driest transformation of the mean streamwise velocity subject to different control measures, in which the density change caused by the compressible effect is taken into account,

$$dU_{VD} = (\overline{\rho}/\overline{\rho}_w)^{1/2} dU, \tag{16}$$

where $U_{VD}^{+} = U_{VD}/u_\tau$, $y^+ = yu_\tau/\nu_w$ and $u_\tau = \sqrt{\tau_w/\rho}$. Note that all the velocities are normalized by the local friction velocity u_τ in each case. It can be seen that the transformed velocity profile in the uncontrolled case conforms to the classical wall law; after the control is applied, the average velocity profile leaves the wall, the buffer zone becomes thicker, the slope κ of the logarithmic law region increases, and the value of the constant C decreases. This is due to that the average density of the inner layer of the boundary layer decreases and the average temperature increases after the control is applied, and the change of the thermodynamic variables directly leads to the change of the flow features of the boundary layer. At the same time, the mean velocity profile away from the wall also indicates that the thickness of the boundary layer increases.

The mean viscous shear stress (*VSS*, defined as $\overline{\mu}(\partial\overline{u}/\partial y)$) and Reynolds shear stress (*RSS*, defined as $(\rho/\rho_w)\overline{u'v'}^{+}$) are compared in Fig. 10, with the *VSS* normalized by the first value of wall in NC. In the near-wall region ($y^+ \leqq 15$), the average viscous shear stress is greatly reduced, which directly leads to the reduction of the skin friction drag. While the region where the Reynolds shear stress is greatly increased is mainly distributed in the logarithmic law region. The above result shows that despite the increase in

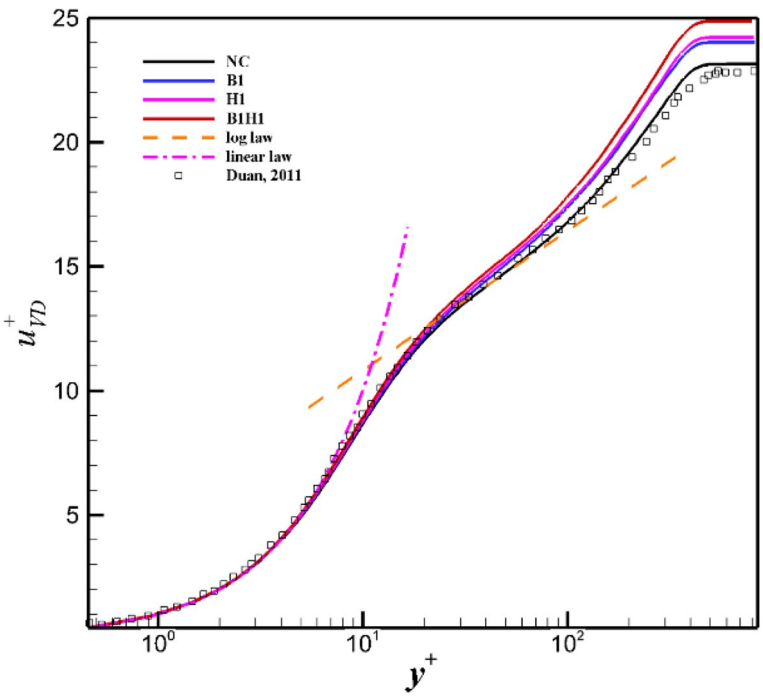

Fig. 9 Profile of van Driest transformed mean velocity obtained at $x = 1150$ mm

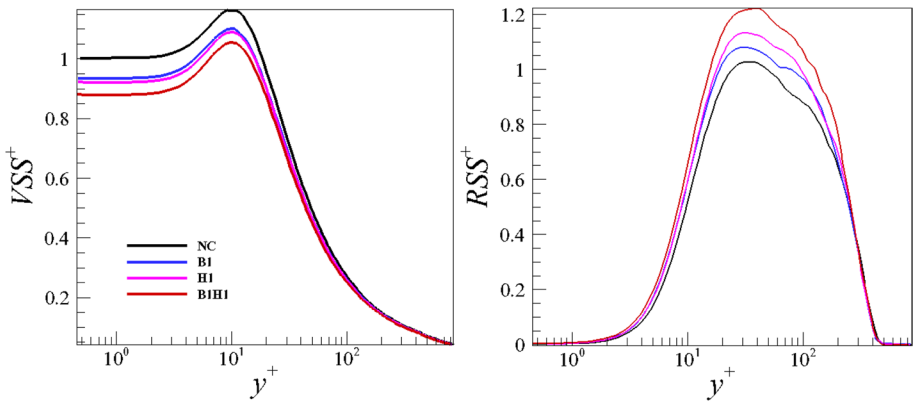

Fig. 10 Mean viscous shear stress and Reynolds shear stress versus inner scaling obtained at $x = 1150$ mm

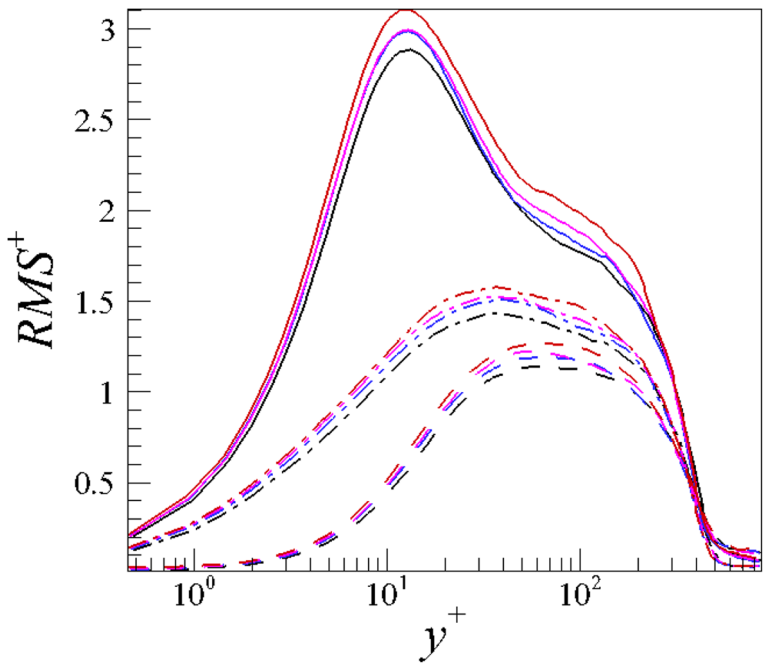

Fig. 11 Turbulence intensities versus inner scaling obtained at $x = 1150$ mm

Reynolds shear stress, the large decrease in mean viscous shear stress near the wall is the direct cause of the decrease in skin friction drag.

The change of turbulence intensities in three directions of each case is plotted versus inner scaling in Fig. 11. RMS^+ in the figure represents the dimensionless turbulence intensities after density weighted transformation, namely $\sqrt{\rho/\rho_w u'^+_{rms}}$, $\sqrt{\rho/\rho_w v'^+_{rms}}$ and $\sqrt{\rho/\rho_w w'^+_{rms}}$, respectively. Similarly, the turbulence intensities in the three directions all increase to varying degrees, indicating that the turbulence amplification effect still exists in the controlled flow field. The maximum turbulence intensities in the streamwise, wall-normal and spanwise directions in B1H1 are increased by 4.06%, 11.02% and 10.25%, respectively, all lower than the growth amplitude under supersonic flow conditions [27]. This means that under the condition of

hypersonic flow, the turbulence amplification effect caused by the flow control method is lower than that under the condition of supersonic freestream, for which the compressibility effect in the hypersonic flow field is stronger.

In order to further analyze the effects of wall blowing and other methods on the Reynolds stress of hypersonic turbulent boundary layer, the following introduces the Lumley triangle [38] to analyze the change of the Reynolds stress anisotropy tensor before and after the control. The anisotropy tensor for Reynolds stress in compressible flow is defined as follows:

$$\boldsymbol{b}_{ij} = \frac{\left\langle \rho u_i'' u_j'' \right\rangle}{\left\langle \rho u_k'' u_k'' \right\rangle} - \frac{1}{3}\delta_{ij}; \tag{17}$$

the second and third invariants are

$$\begin{aligned} II_b &= b_{ij}b_{ji}, \\ III_b &= b_{ij}b_{jk}b_{ki}. \end{aligned} \tag{18}$$

The Reynolds stress anisotropy tensor analysis before and after applying the control is shown in Fig. 12. The x-axis and y-axis in the figure are the third and second invariants of the anisotropy tensor, respectively. In the near-wall region, due to the obstruction of the wall, the Reynolds stress is dominated by two-component turbulence, and its extreme value appears near $y^+ = 6$; as the height increases, the turbulence gradually transforms from axisymmetric expansion to isotropic state, and reaches to an extreme value at about $y/\delta_{99} = 1$. This change indicates the effect of wall constraints on the anisotropy characteristics of Reynolds stress. At the same time, it can be found

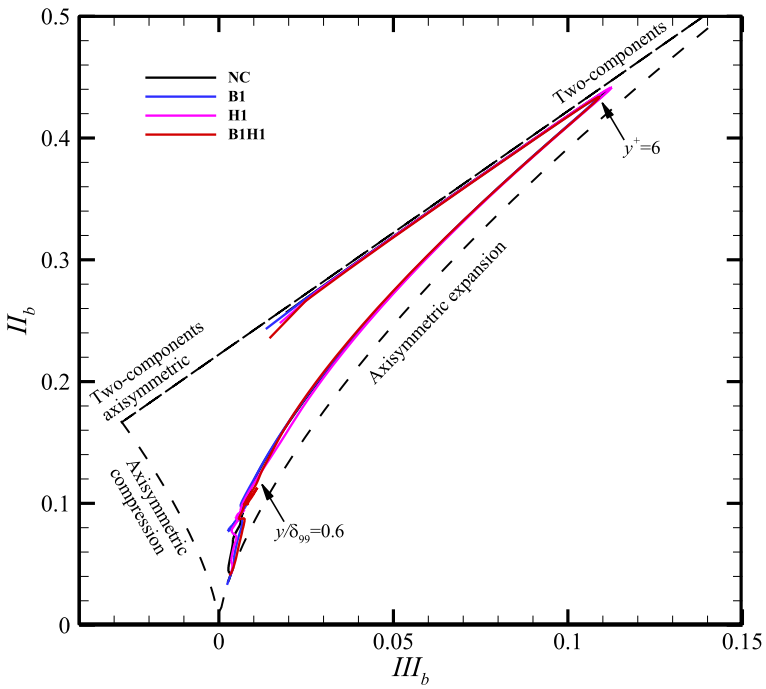

Fig. 12 Anisotropy invariant maps based on (III_b, II_b) obtained at $x = 1150$ mm

that in the Lumley triangle, the Reynolds stress anisotropy characteristics under different flow control measures cannot be found to be significantly different.

In the following, the Barycentric triangle will be introduced to analyze the Reynolds stress anisotropy tensor. Different from the nonlinear mapping in the Lumley triangle described by two invariants of $\boldsymbol{b}_{ij}$, Banerjee et al. [39] proposed to map the tensor $\boldsymbol{b}_{ij}$ in a linear way, namely the Barycentric triangle, which has the advantages of simple transformation and less distortion. By writing the Reynolds stress as

$$\begin{aligned}\boldsymbol{\tau} &= \left\langle \rho u_i u_j \right\rangle = \frac{2}{3} k \delta_{ij} + a_{ij} \\ &= 2k\left(\frac{1}{3}\boldsymbol{I} + \boldsymbol{b}\right) = 2k\left(\frac{1}{3}\boldsymbol{I} + \boldsymbol{V}\boldsymbol{\Lambda}\boldsymbol{V}^T\right),\end{aligned} \tag{19}$$

where $\boldsymbol{I}$ is the second-order identity matrix, $\boldsymbol{V}$ and $\boldsymbol{\Lambda}$ are the corresponding eigenvectors and eigenvalues, $\boldsymbol{\Lambda} = diag[\lambda_1, \lambda_2, \lambda_3]$. Essentially, this form is an eigenvalue decomposition of the tensor $\boldsymbol{b}_{ij}$. Then through the coordinate transformation, the eigenvalues are written in the following form:

$$\begin{aligned}c_1 &= \lambda_1 - \lambda_2, \\ c_2 &= 2 \times (\lambda_2 - \lambda_3), \\ c_3 &= 3\lambda_3 + 1.\end{aligned} \tag{20}$$

Then, the Barycentric triangle can be obtained. Compared with the Lumley triangle, all anisotropic states of the turbulence are enclosed in an equilateral triangle. The geometric meaning of any inner point in the figure is the division of the area of the whole triangle, that is, the area ratio of three triangles formed by connecting the point with the three vertices. Figure 13 shows the Barycentric triangle of the Reynolds stress anisotropy tensor under different control methods. The color of the dots in the figure from red to blue denotes the increase of coordinate height. One can easily find that the influence of different control methods on the Reynolds stress anisotropy tensor is mainly limited to the boundary layer, especially the near-wall region, and the control methods such as wall blowing make the flow in the near-wall region deviate from the two component limit. This may be due to the fact that after the control is applied, the relative activation of wall-normal fluctuating velocity *v*' and the spanwise fluctuating velocity *w*' in the near-wall region increases, and the Reynolds stress in the corresponding direction also increases.

3.3 Flow organization

For the sake of brevity, only the results of the uncontrolled case (NC) and the heated wall blowing control (B1H1) are given for comparison of the turbulent structure characteristics in the following. Figure 14 shows the instantaneous temperature field in streamwise (*x*-*y*) plane. The figures clearly demonstrate that after the heated wall blowing is applied, the overall thickness of the turbulent boundary layer increases. In the near-wall region, the temperature increases while the density decreases, and the change of the thermodynamic variables directly leads to the change of the average flow characteristics.

Vortical structures in the fully turbulent region illustrated by the *Q*-criterion are shown in Fig. 15, where the iso-surface with $Q = 0.2$ is given and colored by the local streamwise velocity. One can find that after the heated wall blowing control is applied,

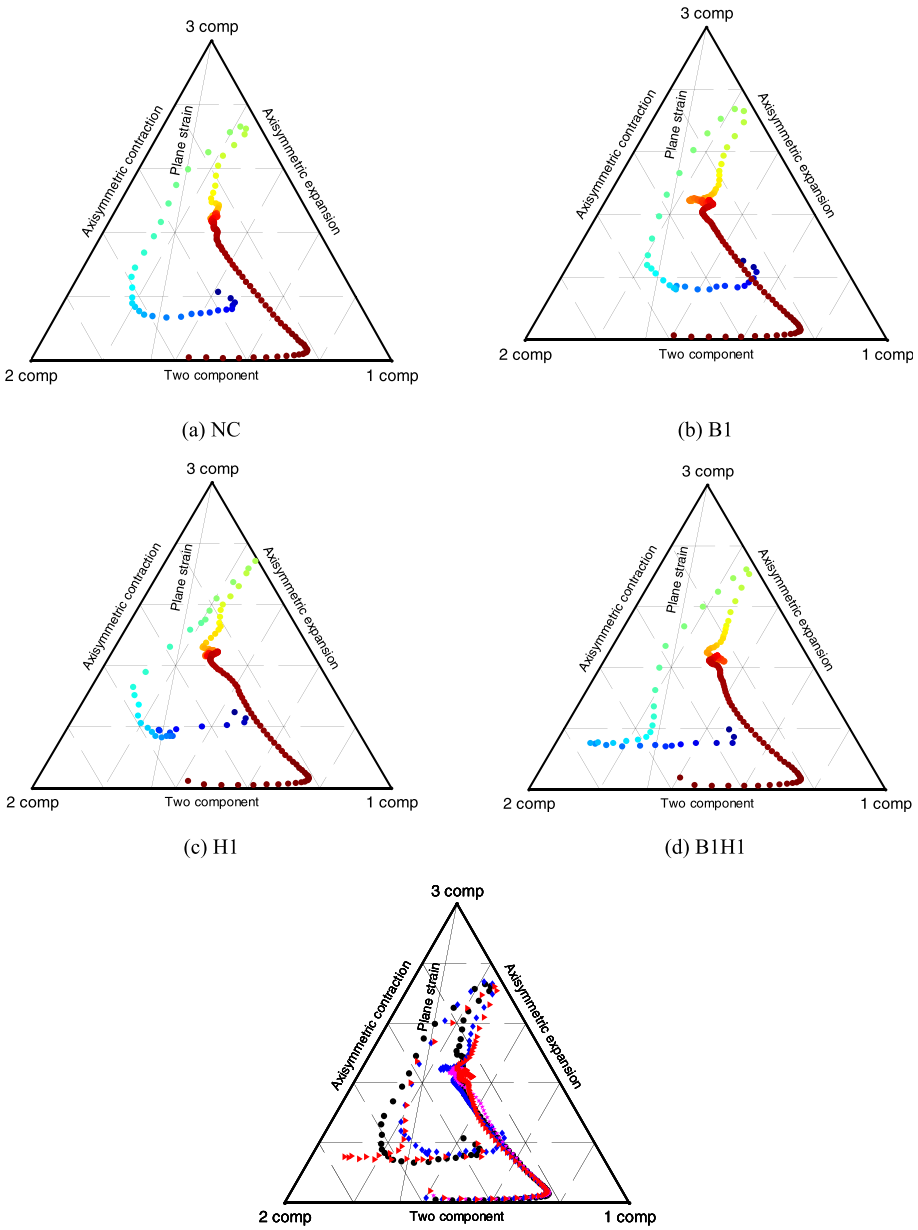

(a) NC (b) B1

(c) H1 (d) B1H1

(e) Comparison

Fig. 13 Barycentric triangle of Reynolds stress anisotropy tensor obtained at $x = 1150$ mm

abundant coherent structures appear, indicating that the small-scale turbulent structures increase, and the turbulence amplification occurs. This is consistent with the results obtained by Kametani et al. [23] in incompressible flow and previous study in supersonic flow [27].

Figure 16 compares the changes of streamwise fluctuating velocity field on the $y^+ = 12$ plane. The velocity range shown in the figure is -0.4 $\leq u' \leq$ 0.4. Obviously, there are numerous high- and low-speed strips alternatingly distributed in the spanwise direction. In B1H1, the areas of extremely high and low fluctuating velocities are significantly

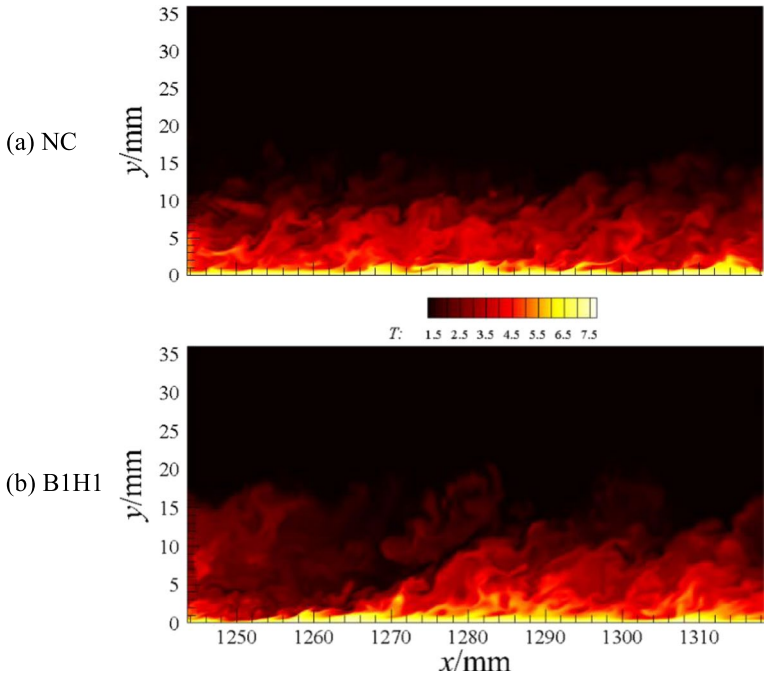

Fig. 14 Temperature contour in streamwise plane under different control methods

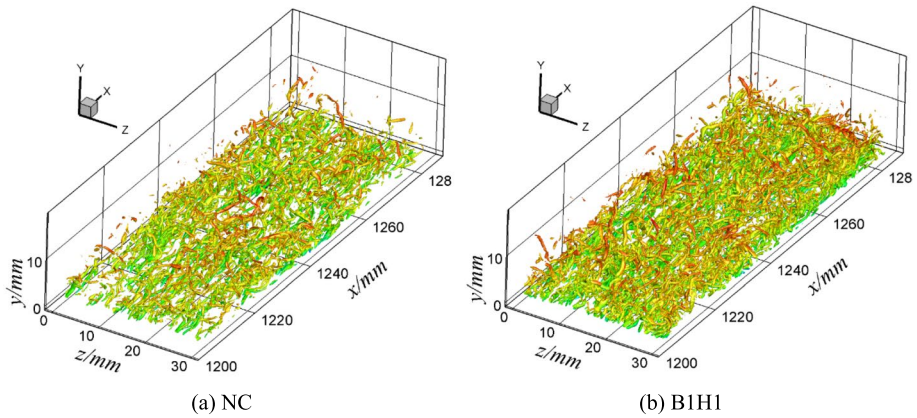

Fig. 15 Iso-surface of $Q = 0.2$ to visualize vortical structures (colored by streamwise velocity)

increased, indicating that the small-scale turbulent structures in the flow field are enhanced and thus the turbulence amplification appears.

Furthermore, two-point spatial correlation is used to quantitatively study the spatial scale change of coherent structure in turbulent boundary layer. The formula is as follows:

$$R_{uu}(x_0 + \Delta x, y_0, z_0 + \Delta z) = \frac{\overline{u'(x_0, y_0, z_0) \cdot u'(x_0 + \Delta x, y_0, z_0 + \Delta z)}}{\sqrt{\overline{u'(x_0, y_0, z_0)^2}} \cdot \sqrt{\overline{u'(x_0 + \Delta x, y_0, z_0 + \Delta z)^2}}}, \tag{21}$$

where the subscript "0" denotes the reference position, which is ($x_0 = 1269$ mm, $z_0 = 15$ mm), and the heights of the wall-normal plane are $y^+ = 12$ and $y^+ = 73$.

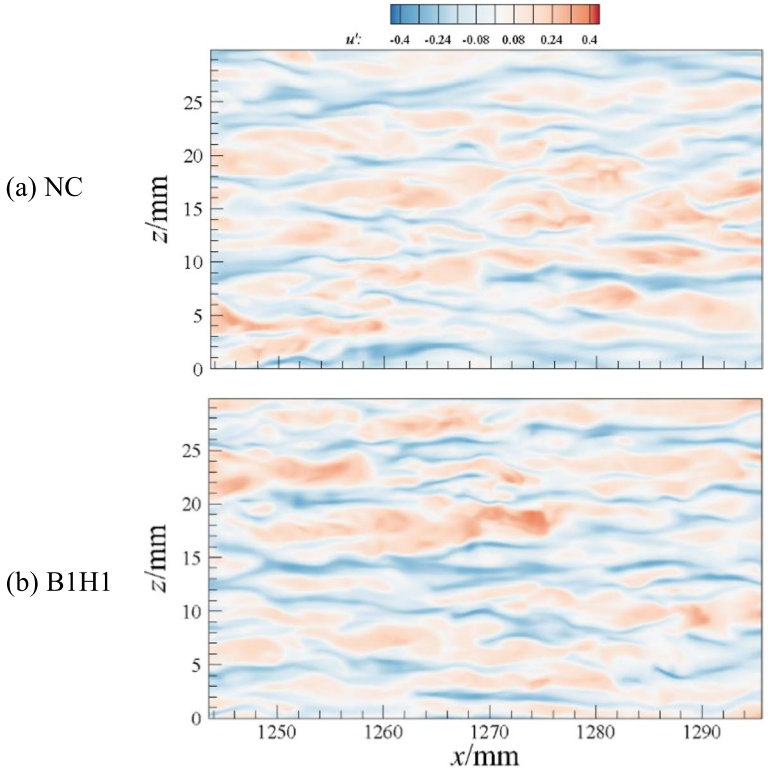

Fig. 16 Instantaneous streamwise velocity fields in wall-parallel plane at $y^+ = 12$ (contour levels are shown for $-0.4 \leq u' \leq 0.4$)

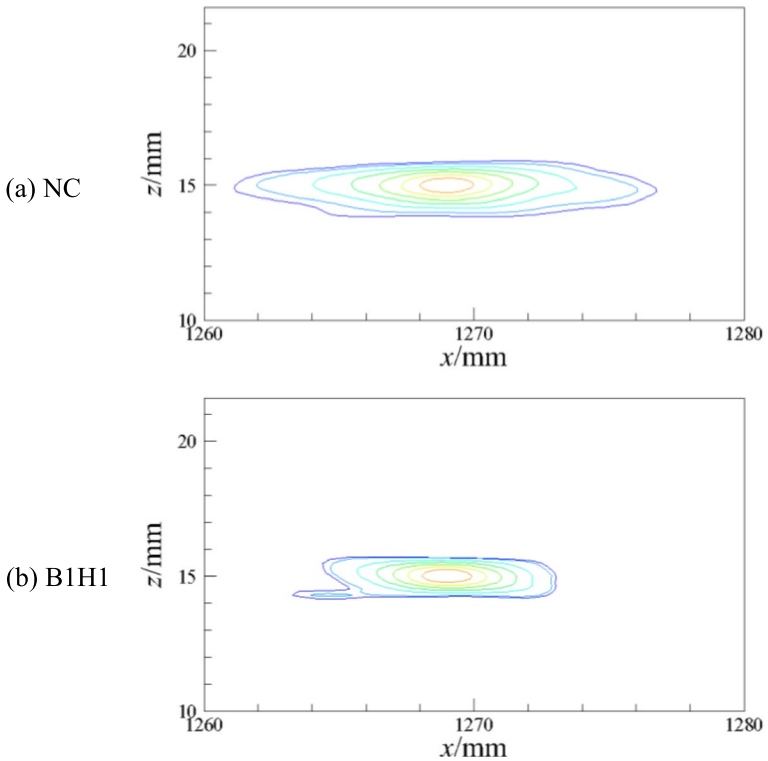

Fig. 17 Two-point correlation coefficient of streamwise fluctuating velocity in *x*-*z* plane at $y^+ = 12$

Figures 17 and 18 show the two-point correlation map of streamwise fluctuating velocity at two wall-normal planes, respectively. It can be easily seen that the spatial scale of the turbulent coherent structures at both heights in the controlled flow field is greatly reduced, almost half of the original one, and the spanwise scale does not change much.

Figure 19 is the results of two-point correlation coefficient in x-y plane. The figure illustrated that after heated wall blowing is applied, the inclination angle of the streamwise vortex in the turbulent boundary layer decreases and the vortex slightly moves away from the wall. The change of the inclination angle of the vortex also explains the internal mechanism of friction drag reduction from the perspective of coherent structure: in the uncontrolled case, the tail part of the streamwise vortex is closer to the wall, which can give continuous counteractions to the wall to a determining extent, resulting in a higher frictional drag. After the flow control is applied, the tail of the streamwise vortex is far away from the wall due to the blowing, the streamwise vortex is lifted and the angle with the wall decreases, so that the interaction between the streamwise vortex and the wall is probably weakened, and the friction drag is reduced accordingly.

All in all, the heated wall blowing control significantly changes the strength and scale of the turbulent coherent structure in the near-wall region. The strength of the streamwise vortex increases while its spatial scale decreases, and the corresponding tail part is lifted away from the wall, effectively weakening the interaction with the wall probably. Thereby, the skin friction coefficient of TBL is reduced.

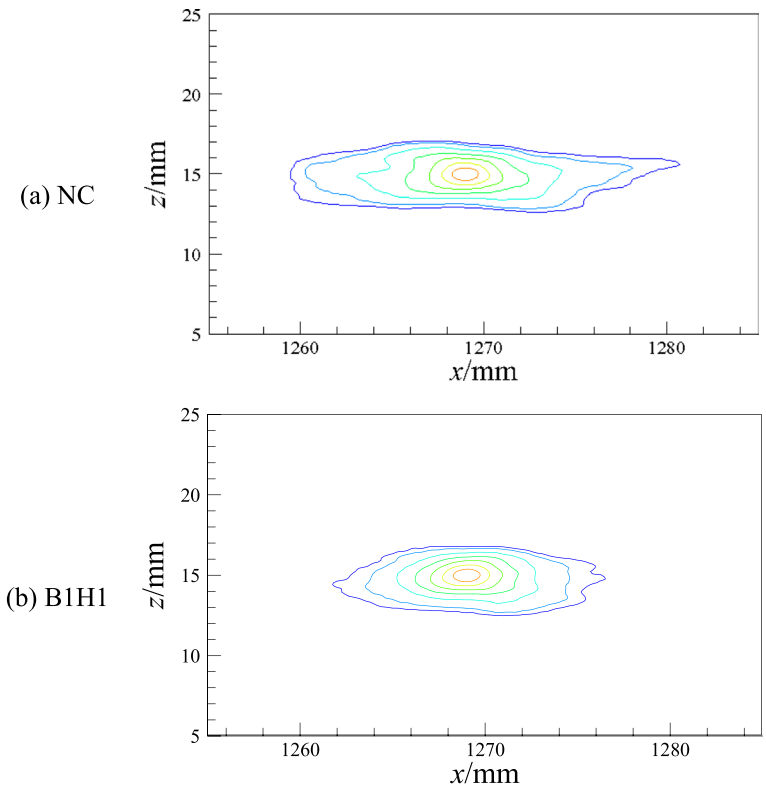

Fig. 18 Two-point correlation coefficient of streamwise fluctuating velocity in x-z plane at $y^+ = 73$

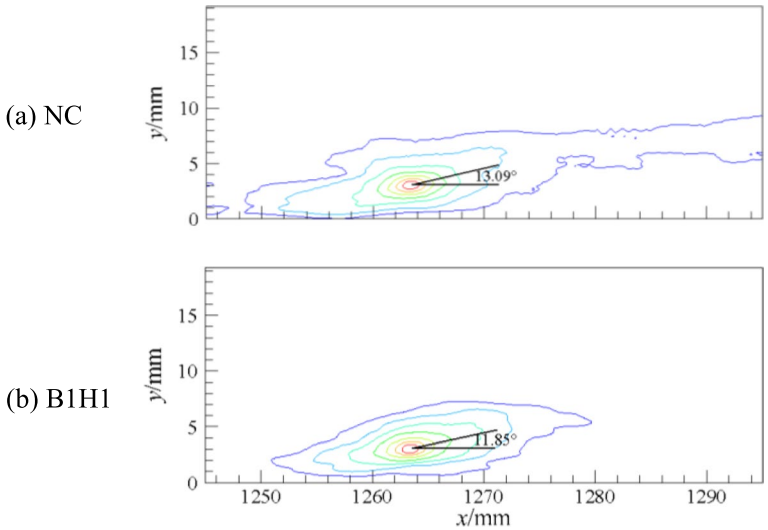

Fig. 19 Two-point correlation coefficient of streamwise fluctuating velocity in *x*-*y* plane

4 Conclusions

Turbulence drag reduction in hypersonic flows is a hot topic in both fundamental study and aeronautical engineering. In this paper, the proposed velocity-temperature coupled drag reduction control method is further extended to a Mach 6 hypersonic turbulent boundary layer. Comparative analysis of TBL subject to wall blowing, wall heating and heated wall blowing is studied by direct numerical simulations.

The results show that in the hypersonic flow, the drag reduction rate of velocity-temperature coupling control is 10.58%, about the sum of that in wall blowing (5.27%) and wall heating (6.35%). However, the control efficiency is greatly reduced. The decrease in drag reduction rate is due to the stronger compressibility effect of the flow field, while the decrease in control efficiency is due to the higher energy consumption required for the heated wall blowing with an ejection temperature to $1.01T_w$ under hypersonic conditions. Therefore, when using heated wall blowing, the energy consumption required to heat the blowing gas should be carefully considered. To clarify the drag reduction mechanism, the modified FIK decomposition of skin friction coefficients is introduced, and it is found that the sharp reduction of the mean convection term is the main reason for the reduction of the turbulence drag.

Results of van Driest transformation of the mean streamwise velocity indicate that the thickness of the boundary layer increases, the viscous sublayer and the buffer layer become thicker, and the logarithmic law region moves off the wall. The reduction of the mean viscous shear stress is the direct reason for the drag reduction, although the Reynolds shear stress is enhanced. The anisotropic invariant of Reynolds stress is further studied, and it is found that the applied flow control method only affects the Reynolds stress in the near-wall region, and the corresponding turbulent state tends to be more isotropic. The turbulence amplifications can be attributed to the enhancement of coherent structures, which can be reflected by the Q-criterion. The heated wall blowing brings about abundant coherent structures. Those structures are found to be in small scales and slightly away from the wall as shown by the two-point spatial correlation.

Future work will pay attention to obtaining the net energy saving rate of velocity-temperature coupling control measures in hypersonic TBL. On one hand, it can be achieved by reducing the amplitude of the blowing temperature. 1% amplitude in temperature increment in this paper is so large as to require high energy consumption. Reducing it by one order of magnitude may result in an expected net energy saving rate. On the other hand, the velocity amplitude of wall blowing can be further improved to get higher gains.

Acknowledgements
The authors gratefully acknowledge Prof. X.L. Li in Institute of Mechanics, Chinese Academy of Sciences for providing OpenCFD software and valuable support. The National Supercomputing Center in Beijing is also acknowledged for providing supercomputer time.

Authors' contributions
Our group has been working on the topic for a long time. The research output comes from our joint efforts. All authors read and approved the final manuscript.

Funding
The present study is supported by the National Natural Science Foundation of China (Grant Nos. 12202488 and 12072306), Natural Science Program of NUDT (ZK22-30) and Independent Cultivation Project for Young Talents of the College of Aerospace Science and Engineering.

Availability of data and materials
The data that support the findings of this study are available from the corresponding author upon reasonable request.

Declarations

Competing interests
The authors declare that they have no competing interests.

Received: 31 October 2022 Accepted: 27 December 2022
Published online: 21 February 2023

References

1. White FM (1974) Viscous fluid flow. McGraw-Hill Higher Education, New York
2. Gad-el-Hak M (2000) Flow control: Passive, active, and reactive flow management. Cambridge University Press, Cambridge
3. Duan L, Choudhari MM (2012) Effects of riblets on skin friction and heat transfer in high-speed turbulent boundary layers. Paper presented at the 50th AIAA aerospace sciences meeting including the new horizons forum and aerospace exposition, Nashville, 9-12 January 2012
4. Ye LQ, Ye ZY, Ye K et al (2021) A low-boom and low-drag design method for supersonic aircraft and its applications on airfoils. Adv Aerodyn 3:25
5. Cui G, Pan C, Wu D et al (2019) Effect of drag reducing riblet surface on coherent structure in turbulent boundary layer. Chinese J Aeronaut 32(11):2433–2442
6. Zhang Y, Ye ZX, Li BH et al (2022) Numerical analysis of turbulence characteristics in a flat-plate flow with riblets control. Adv Aerodyn 4:29
7. Suzuki Y, Kasagi N (1994) Turbulent drag reduction mechanism above a riblet surface. AIAA J 32(9):1781–1790
8. Choi H, Moin P, Kim J (1993) Direct numerical simulation of turbulent flow over riblets. J Fluid Mechanics 255:503–539
9. Robinson SK (1988) Effects of riblets on turbulence in a supersonic boundary layer. AIAA Paper 1988-2526
10. Gaudet L (1989) Properties of riblets at supersonic speed. Appl Sci Res 46:245–254
11. Coustols E, Cousteix J (1994) Performances of riblets in the supersonic regime. AIAA J 32(2):431–433
12. Duan L, Choudhari MM (2014) Direct numerical simulations of high-speed turbulent boundary layers over riblets. Paper presented at the 52nd aerospace sciences meeting, National Harbor, 13-17 January 2014
13. Chen Z (2016) Numerical study of drag reduction in compressible wall-bounded turbulence. Dissertation, University of Chinese Academy of Sciences
14. Zhou H, Li XL, Yu CP (2020) Study on turbulence drag reduction of riblet plate in hypersonic turbulent flows. Int J Mod Phys C 31(3):2050046
15. Kametani Y, Kotake A, Fukagata K et al (2017) Drag reduction capability of uniform blowing in supersonic wall-bounded turbulent flows. Phys Rev Fluids 2(12):123904
16. Chen Z, Yu CP, Li L et al (2016) Effect of uniform blowing or suction on hypersonic spatially developing turbulent boundary layers. Sci China Phys Mech Astron 59(6):664702
17 Duan L, Beekman I, Martin MP (2010) Direct numerical simulation of hypersonic turbulent boundary layers. Part 2. Effect of wall temperature. J Fluid Mech 655:419–445
18. Huang JJ, Nicholson GL, Duan L et al (2020) Simulation and modeling of cold-wall hypersonic turbulent boundary layers on flat plate. Paper presented at the AIAA scitech 2020 forum, Orlando, 6-10 January 2020

19. Liang X, Li XL (2015) Direct numerical simulation on Mach number and wall temperature effects in the turbulent flows of flat-plate boundary layer. Commun Comput Phys 17(1):189–212
20. Morkovin MV (1962) Effects of compressibility on turbulent flow. In: Favre AJ (eds) Mécanique de la Turbulence, CNRS, Paris, pp 367-380
21 Li X, Tong FL, Yu CP et al (2020) Correlation between density and temperature fluctuations of hypersonic turbulent boundary layers at $Ma_\infty = 8$. AIP Adv 10(7):075101
22. Xu DH, Wang JC, Wan MP et al (2021) Compressibility effect in hypersonic boundary layer with isothermal wall condition. Phys Rev Fluids 6(5):054609
23. Kametani Y, Fukagata K (2012) Direct numerical simulation of spatially developing turbulent boundary layer for skin friction drag reduction by wall surface-heating or cooling. J Turbul 13(34):1–20
24. Zhang Z, Tao Y, Xiong N et al (2018) The effect of wall temperature distribution on streaks in compressible turbulent boundary layer. Mod Phys Lett B 32(12n13):1840051
25. Hickey JP, Younes K, Yao MX et al (2020) Targeted turbulent structure control in wall-bounded flows via localized heating. Physics of Fluids 32(3):035104
26. Liu Q, Luo ZB, Wang L et al (2021) Direct numerical simulations of supersonic turbulent boundary layer with streamwise-striped wall blowing. Aerosp Sci Technol 110:106510
27 Liu Q, Luo ZB, Tu GH et al (2021) Direct numerical simulations of a supersonic turbulent boundary layer subject to velocity-temperature coupled control. Phys Rev Fluids 6(4):044603
28. Renard N, Deck S (2016) A theoretical decomposition of mean skin friction generation into physical phenomena across the boundary layer. J Fluid Mech 790:339–367
29 Pirozzoli S, Grasso F (2004) Direct numerical simulation and analysis of a spatially evolving supersonic turbulent boundary layer at M=2.25. Phys Fluids 16(3):530–545
30. Li XL, Fu DX, Ma YW et al (2010) Direct numerical simulation of compressible turbulent flows. Acta Mech Sin 26:795–806
31. Dong SW, Tong FL, Yu M et al (2022) Effects of wall temperature on two-point statistics of the fluctuating wall shear stress and heat flux in supersonic turbulent boundary layers. Phys Fluids 34(6):065114
32. van Driest ER (1956) The problem of aerodynamic heating. Aeronaut Eng Rev 15:26–41
33. Smits AJ, Matheson N, Joubert PN (1983) Low-Reynolds-number turbulent boundary layers in zero and favorable pressure gradients. J Ship Res 27(3):147–157
34. Roy CJ, Blottner FG (2006) Review and assessment of turbulence models for hypersonic flows. Prog Aerosp Sci 42(7-8):469–530
35. Nagib HM, Chauhan KA, Monkewitz PA (2007) Approach to an asymptotic state for zero pressure gradient turbulent boundary layers. Phil Trans R Soc A 365:755–770
36. Choi H, Moin P, Kim J (1994) Active turbulence control for drag reduction in wall-bounded flows. J Fluid Mech 262:75–110
37. Xu J, Dong SC, Maxey MR et al (2007) Turbulent drag reduction by constant near-wall forcing. J Fluid Mech 582:79–101
38. Lumley JL, Newman GR (1977) The return to isotropy of homogeneous turbulence. J Fluid Mech 82(1):161–178
39. Banerjee S, Krahl R, Durst F et al (2007) Presentation of anisotropy properties of turbulence, invariants versus eigenvalue approaches. J Turbul 8(32):1–27

Publisher's Note

Springer Nature remains neutral with regard to jurisdictional claims in published maps and institutional affiliations.

Submit your manuscript to a SpringerOpen journal and benefit from:

- ► Convenient online submission
- ► Rigorous peer review
- ► Open access: articles freely available online
- ► High visibility within the field
- ► Retaining the copyright to your article

Submit your next manuscript at ► springeropen.com